Design of a Device for the Automated Mapping, and Treatment of Atrioventricular Nodal Reentry Tachycardia

by Erdit Gremi

B.S. in Biomedical Engineering, December 2013, Georgia Institute of Technology

A Thesis submitted to

The Faculty of
The School of Engineering and Applied Science
of the George Washington University
in partial fulfillment of the requirements
for the degree of Master of Science

January 19, 2018

Thesis directed by

Igor Efimov
Alisann and Terry Collins Professor of Biomedical Engineering

© Copyright 2017 by Erdit Gremi
All rights reserved

Dedication

The author wishes to dedicate this to Nona who passed away before she had a chance to see what her grandson was learning in school today.

Acknowledgments

The author wishes to thank Professor Efimov for the time and support he provided throughout the entire thesis project, and to Kedar Aras for all his assistance in the lab and lessons throughout the process.

Abstract of Thesis

Design of a Device for the Automated Mapping, and Treatment of Atrioventricular Nodal Reentry Tachycardia

The technologies introduced in this thesis are developed by Dr. John Roger's lab at the University of Illinois Urbana in collaboration with the Igor Efimov lab at George Washington University. The novel technologies enable a robust set of tools and platforms which makes it possible to design a host of devices for the improved treatment of disease states. This document will focus on the applications of this technology on Atrioventrivular Nodal Reentry Tachycardia as it is a disease state that is well understood, prevalent in the population, and lends itself to the application of new technologies to improve treatment outcomes. The thesis will describe the clinical significance, and pathophysiology of Atrioventricular Nodal Reentry Tachycardia, examine the current state of clinical practice for how the disease is treated and with what devices it is treated. This document will also evaluate the constraints present in current technologies and introduce new technologies with promise of new treatment options highlighting the new capabilities that such new technologies give rise to and the new limitations that come with them. Finally, this thesis will propose a novel device to be used in the treatment of AVNRT. The proposal will document the requirements for that device, and provide a design specification for how to achieve those requirements. This thesis is accompanied by a provisional design patent for the use of the novel technologies and the utilization of the new technologies in a wider set of possible embodiments. The work contained in this thesis serves as a detailing of one particular embodiment of a device.

Table of Contents

Dedication iii

Acknowledgments iv

Abstract of Thesis v

List of Figures viii

Chapter 1: Introduction 1

1.1 Background 1

1.2 Anatomy 1

1.2.1 Biochemical Anatomy 2

1.2.2 Electrophysiology 4

1.3 Clinical Practice 6

Chapter 2: State of the Art and Proposal 6

2.1 Literature Review 9

2.2 Innovation 12

2.2.1 Utilization in Balloon Catheter 13

2.2.2 Chiplet Technology for Mapping 14

2.2.3 Ablation and Pacing Electrodes 17

2.2.4 In-vitro Electrical Performance 19

2.2.5 Animal Model Performance 21

Chapter 3: Methods 11

3.0 Proposal 23

3.1 Design Requirements 24

3.2 Characterize ToK Anatomical Differences 24

3.2.1 Quantitative Analysis of Dimensions 28

3.3 Electrode Layout 29

3.4 Deployment Mechanism 33

3.5 Anchoring Mechanism 34

3.6 Design Specifications 34

3.7 Comparison of Workflow 36

3.8 Patent Generation 37

Chapter 4: Conclusion 41

4.1 Discussion 41

4.2 Future Work 41

Bibliography 45

List of Figures

Figure 1…….2

Figure 2…….3

Figure 3…….5

Figure 4…….6

Figure 5…….....9

Figure 6…….....11

Figure 7……..……...12

Figure 8……..……...14

Figure 9……..……...16

Figure 10..……18

Figure 11..……20

Figure 12..……22

Figure 13..……25

Figure 14..……26

Figure 15..……27

Figure 16..……29

Figure 17..……30

Figure 18..……32

Figure 19..……36

Figure 20..……37

Chapter 1 – Introduction

1.1 Background

An arrhythmia is a disorder with the speed or rhythm of the heartbeat. Aberrant conductive pathways disrupt the normal path of the heart's electrical impulses. For example, conduction blocks can cause the electrical impulse to degenerate into circular wavelets that disrupt the normal activation of the atria or ventricles. In patients with cardiac arrhythmias, abnormal regions of cardiac tissue do not follow the synchronous beating cycle associated with normally conductive tissue in patients with sinus rhythm. Instead, the abnormal regions of cardiac tissue aberrantly conduct to adjacent tissue, thereby disrupting the cardiac cycle into an asynchronous cardiac rhythm. Such abnormal conduction has been previously known to occur at various regions of the heart, such as, for example, along the conduction pathways of the atrioventricular node (AVN) and the Bundle of His (BoH). Atrioventricular nodal reentrant tachycardia (AVNRT), is a type of abnormal fast heart rhythm which occurs when a reentry circuit forms within or just next to the AVN. It is a type of supraventricular tachycardia (SVT), which is defined as an arrhythmia that originates from a location within the heart above the BoH.[1]

1.2 Anatomy

The AVN is located in the paraseptal endocardium of the right atrium (RA), at the junction of the Triangle of Koch (ToK), formed by the ostium of the coronary sinus (CS), the tendon of Todaro (TT), and the tricuspid valve (TV).[1] The AVN can further be categorized into the lower nodal bundle (LNB) and compact node (CN).

From the LNB, the rightward inferior nodal extension (INE) spreads along the atrial annulus of the TV towards the CS and the leftward nodal extension spreads from the CN along the TT.[2]

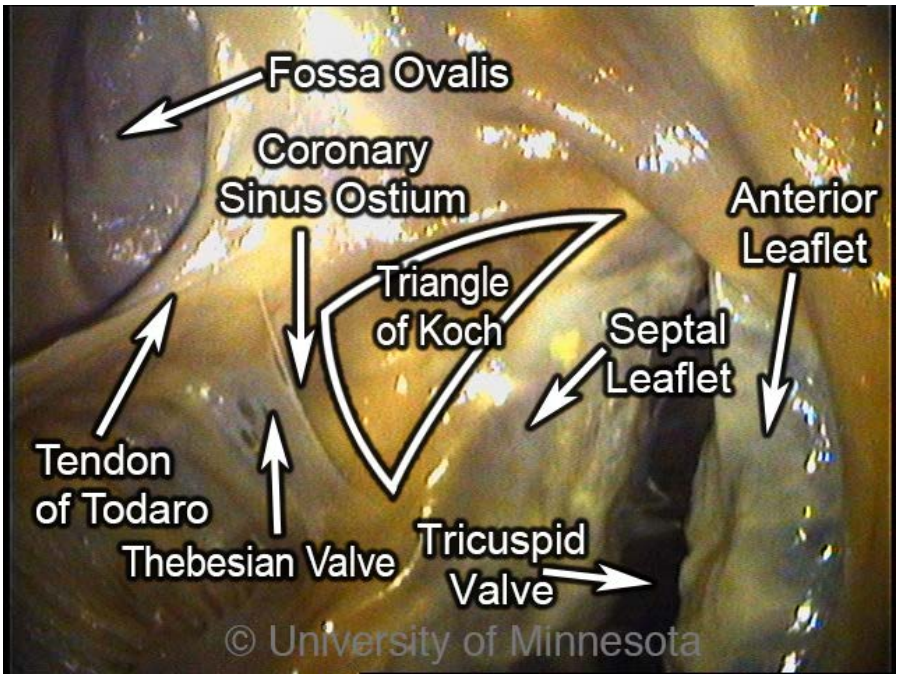

***Figure 1**: Diagram of Triangle of Koch boundary (Figure from University of Minnesota Atlas of Human Cardiac Anatomy)[3]*

1.2.1 Biochemical Anatomy

Electrical coupling between cells occurs via gap junctions which create pores between neighboring myocytes and facilitate the electrical and chemical signals between the them. The gap junctions are hexameric protein structures formed by connexins (Cx) and vary in conductance based on the Cx isoforms.[4-6] The most commonly expressed isoforms in the AVN are Cx40 (which have large conductance) and Cx43 (medium conductance).[7] The AVN has a distinct distribution of these connexin isoforms that promote its physiological functions. Various studies have

characterized total protein and mRNA levels of Cx40, and Cx43 qualitatively and quantitatively in the human AVN.[8-10] Representative Cx43 immunolabelled sections are shown in Figure 2B, alongside their serially sectioned histological images Figure in 2A.

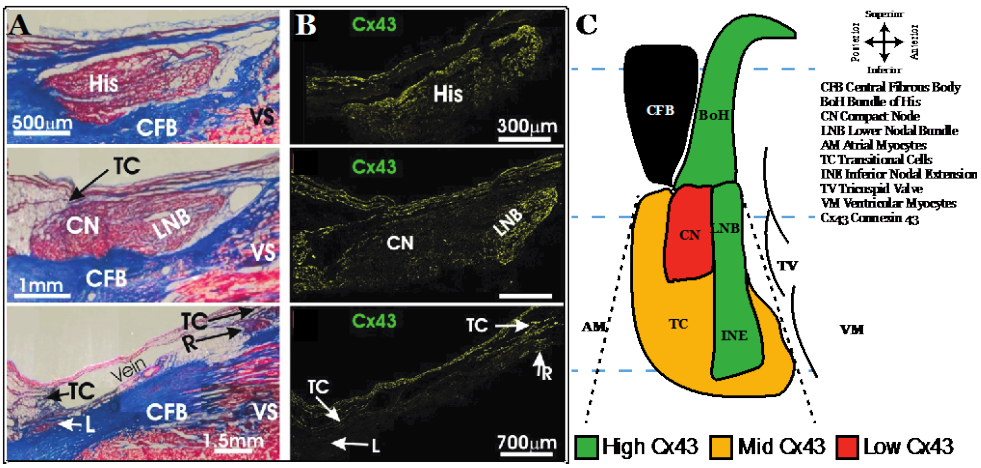

Figure 2: *Serial sections processed for histology (A) and Cx43 immunolabelling (B) from the human AVN taken from three separate planes. These planes of sectioning are indicated by the blue lines in the Cx43 expression profile schematic (C)(Figures from Hucker. et al.)[10]*

Atrial myocytes (AM) strongly express both Cx43 and Cx40 proteins and mRNA. The BoH, and Left Nodal Bundle (LNB) have both high Cx40 and Cx43 levels. [8-10] Cx43 and Cx40 are also expressed in the proteins and mRNA of transitional cells (TC), but at lower levels. Conversely, the compact node, has elevated Cx40 expression but very low Cx43. The INE has high Cx43 expression but reduced Cx40. The expression profile for Cx43 in the human AVN is shown in Figure 2C. Generally, Cx40 and Cx43 can be thought to be expressed in opposite levels in tissues of the AVN (high Cx43, means low Cx40 and vise-versa) except for the BoH and LNB where they are both present in elevated levels.

1.2.2 Electrophysiology

Electrophysiological refractoriness defines the time interval after an action potential where the cell cannot be re-excited. Studies have shown that the tissues of the SP have a shorter refractory period than those of the FP.[11, 12]

The AVN serves as the pathway for electrical excitation between the atria and ventricles. Due to its protein expression profiles, the conduction of electrical excitation is slow in the AVN relative to the working myocardium.[13] There are also conduction velocity differences even within the compartments of the AVN. [13-15] The tissue heterogeneities described above drive these differences and create the FP and SP pathways of AVN conduction. During a normal beat, atrial excitation occurs prior to AVN excitation as shown in Figure 3B (Left). The conduction wavefront moves through the AVN, anterogradely through both the FP and SP (Figure 3B, Middle). The wave reaches the BoH earlier through the FP relative to the SP. BoH activation then (Figure 3B, Right) ventricular activation occur afterwards.[13] Fast and Slow pathway does not refer to the conduction velocity through these structures. The terminology arises from the conduction delay through these structures. It takes longer for excitation to reach the BoH through the SP due to its larger anatomic length. Conversely, conduction velocity is slower through the FP but due to it shorter length, excitation reaches the BoH first through this pathway.[16]

Abnormal activation sequences or rhythms through this complex nodal structure can result in the development of a re-entrant rotor within the dual conduction pathway of the AVN. This then gives rise to arrhythmias such as AVNRT.[13] A diagram of the

AVN during an SP-FP AVNRT episode is demonstrated in Figure 3A where the wavefront propagates retrogradely up the FP and then anterogradely through the SP.

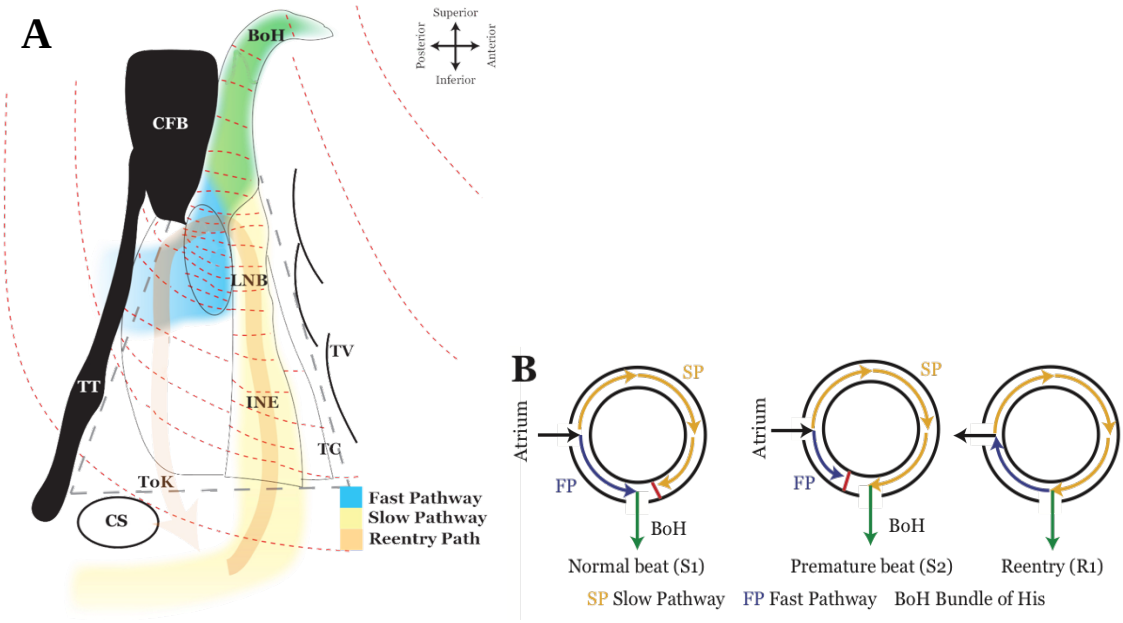

***Figure 3A**: Summary of the various anatomical structures that constitute the AVN and its dual conduction pathways, FP (blue) and SP (yellow). Dashed red lines indicate speed of conduction through the various structures, closely spaced lines indicate slower conduction velocity and vice versa. SP-FP reentrant pathway highlighted by orange arrow. TT – tendon of Todaro, CS – coronary sinus, ToK – Triangle of Koch, CFB – Central Fibrous Body, CN – Compact Node, BoH – Bundle of His, LNB – Lower Nodal Bundle, INE – Inferior Nodal Extension, TV – Tricuspid Valve, VM – ventricular myocytes. B: Dual pathways of electrical wavefront propagation between atria and His Bundle during normal beat (Left) and during a premature beat resulting in a reentrant arrhythmia (Right).(Figures from Sharon A. George, Department of Biomedical Engineering, The George Washington University)*

Slow/Fast AVNRT is the most typical type of AVNRT and occurs when a premature atrial complex (PAC) travels antegradely down the SP (right inferior extension) between the Coronary Sinus ostium and the tricuspid annulus followed by retrograde conduction along the FP.

Fast/Slow AVNRT is more atypical than Slow/Fast and occurs when antegrade conduction occurs down the fast pathway and retrograde conduction occurs up the right inferior extension (slow pathway) with earliest atrial activation at the inferior

septum. Occasionally retrograde conduction occurs up the left inferior extension (leftward slow pathway).

There is a third, but rare AVNRT type called Slow/Slow. In general, Slow/Slow AVNRT conduction occurs antegradely down the rightward inferior extension and retrogradely up the leftward inferior extension. The earliest retrograde atrial activation is therefore often the roof of the coronary sinus although it may also be between the coronary sinus and the tricuspid annulus if retrograde conduction occurs along the rightward inferior extension.

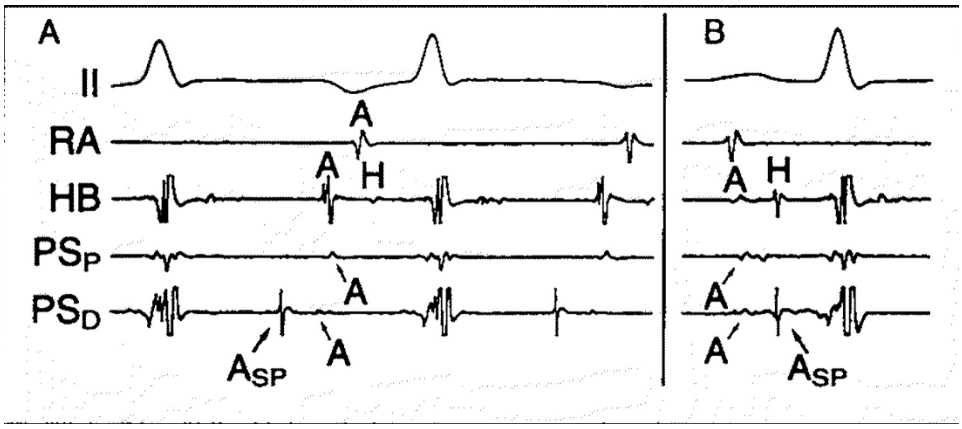

Figure 4*: From the top, the figure shows a tracing from Lead II and ECGs recorded from the right atrial appendage (RA), the His-bundle region (HB), and the proximal (PSP) and distal (PSD) pairs of electrodes of the mapping catheter, positioned against the right atrium between the coronary-sinus ostium and the tricuspid annulus. During fast—slow AVNRT (Panel A), retrograde conduction occurred over the slow pathway, and the earliest retrograde atrial potential was recorded from the PSD electrodes, which showed a small atrial potential (A), nearly coincident with the atrial potentials in the PSP and HB ECGs. It was preceded by a large ASP potential (large arrow) recorded 60 msec before the onset of the P wave. During sinus rhythm (Panel B), when the slow pathway was activated in the antegrade direction, the order of the two potentials in PSD was reversed, with the A potential still coincident with the other atrial potentials. The application of radiofrequency current at this site eliminated antegrade and retrograde slow-pathway conduction and both forms of AVNRT. H denotes His-bundle potential. (Figure from Jackman et al.)*[18]

1.3 Clinical Practice

Ablation is one way of treating AVNRT and restoring normal electrical conduction and contraction. A cardiac ablation procedure begins with mapping the electrical activity of a treatment site prior to permanent ablation, in order to pinpoint

appropriate ablation target sites. Some apparent target sites may not actually contribute to abnormal electrical activity, and treating such sites is not desirable because doing so may affect healthy tissue in undesirable ways (e.g., creating conduction blocks). The cardiac cell is typically 100-150 micron in length and 15-20 microns in width.[21] Thus, precisely mapping the electrical activity in a target treatment region can help focus the treatment and confirm its efficacy and safety.

A specialized catheter is used to electrically map cardiac tissue, such as a circular catheter. Such a mapping catheter is positioned at possible treatment sites inside a patient, and mapping electrodes at those sites can provide signals to a processing system external to the patient that can process the signals and provide physicians with information to subsequently provide therapy. Traditional mapping catheters gather electrical information about a single point on the endocardium.

After mapping, the physician may proceed to ablate the aberrant tissue. In radio-frequency (RF) ablation, RF energy is directed from the ablation electrode through tissue to an electrode to ablate the tissue and form a lesion at the slow pathway. Radiofrequency current (550 to 750 kHz) is commonly delivered at 45 to 70 V between the catheter-tip electrode and an adhesive electrosurgical dispersive pad applied to the left posterior chest. Current is applied for 45 seconds or longer but is terminated immediately if there is an increase in impedance or displacement of the catheter electrode.

Upon the completion of the ablation procedure, the physician applies electrical pacing rhythm to the region of interest so that the electrophysiological pacing of an aberrant heart may be initiated. This pacing energy is supplied by another catheter

and is done to ensure that the ablation procedure has been successful in eliminating any aberrant electrical pathways in the cardiac tissue of interest. The most common way is through the introduction of atrial or ventricular pre-mature depolarization beats. Continuous burst pacing or rapid incremental pacing to 135% of the Tachycardia pace at 5V in the RA or the coronary sinus may induce the tachycardia.[20]

If the pacing electrode is successful in initiating an arrhythmia in the cardiac tissue, the physician will further map and ablate the cardiac tissue till until an arrhythmia can no longer be generated in the cardiac tissue. If the pacing electrode is not successful in initiating an aberrant rhythm in the cardiac tissue, the physician will conclude the ablation procedure.

This process of using a mapping catheter to find the aberrant tissue, switching to an ablation catheter, using an ablation catheter to ablate tissue, switching to a pacing catheter, using the pacing catheter to generate another arrhythmia is time consuming and highly dependent on the skill of a trained physician. Additionally, the repeated switching to different catheters introduces difficulty of targeting an exact location that has been mapped because the patient heart is still beating and the motion introduces additional difficulty in operation. Additionally, mapping single points of the endocardium can extend the length of a procedure if the physician is not able to find the aberrant tissue or if the aberrant tissue is localized to a small area of the heart.[1]

Chapter 2: State of the Art

2.1 Literature Review

The current manifestations of devices used to diagnose, map and pace the electrical rhythms of the heard are limited in their specificity of function and their low resolution in providing information to the physician.

Mapping catheters on the market are often designed as steerable and formable shafts with a single electrode on the distal end of the electrode shaft, or with multiple electrodes on the surface of the mapping catheter shaft in the distal region of the device to detect electrical signals of the desired tissue. The limited surface area of a thin catheter shaft inherently limits the number of electrodes that can be placed on its surface.[21-23] This results in traditional mapping catheters with a low number of mapping electrodes with which to diagnose aberrant signal pathways in the tissue.

Figure 5a-d

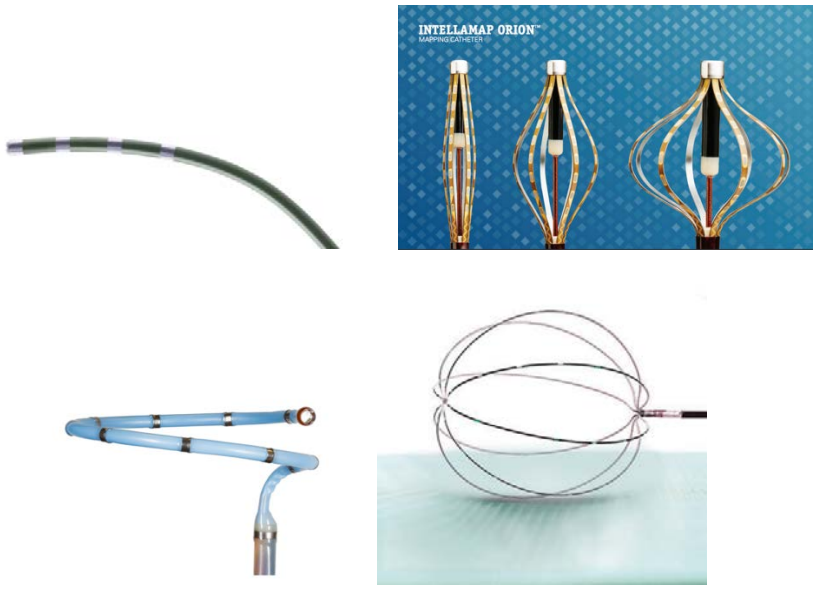

Figure 5 *Top Left: Boston Scientific 4 electrode mapping catheter.[19] Top Right: Boston Scientific Orion 64 electrode mapping catheter[19] Bottom Left: Biosense Webster 12 electrode mapping catheter[23] d) Bottom Left: Abbot 64 electrode mapping catheter[24](Figures from respective company's product catalog)*

New designs such as the FIRMap Catheter (Figure 5d) by Abbott has a total of 64 evenly spaced electrodes, distributed between 8 splines (8 electrodes per spline) in what is known as a basket catheter. The spline design facilitates deployment of electrodes across the chamber thus providing more resolution for atrial endocardium mapping purposes.

The design of pacing catheters is limited to a single pacing electrode on the distal end of an electrode shaft to be applied separately from the mapping catheter during the diagnostic procedure. Similarly to mapping catheters, RF ablation catheters on the market are often designed as steerable and formable shafts with a single ablation electrode on the distal end of the electrode shaft, or with multiple ablation electrodes on the surface of the mapping catheter shaft in the distal region of the ablation catheter to deliver the ablation energy to the desired tissue.[24-26] The standard ablation catheter is 6 French (2mm in diameter) and operates at anywhere from 0.3W to 9.3 Watts.[27] Lesion size is determined by contact length, and power delivery but is limited from 0 to 8.3mm in diameter and is accepted to occur when the tissue temperature is at 45˚C.[28] Ablation catheters may incorporate irrigation systems for the purpose of cooling the tissue that is adjacent to the location where ablation energy is being applied. [19]

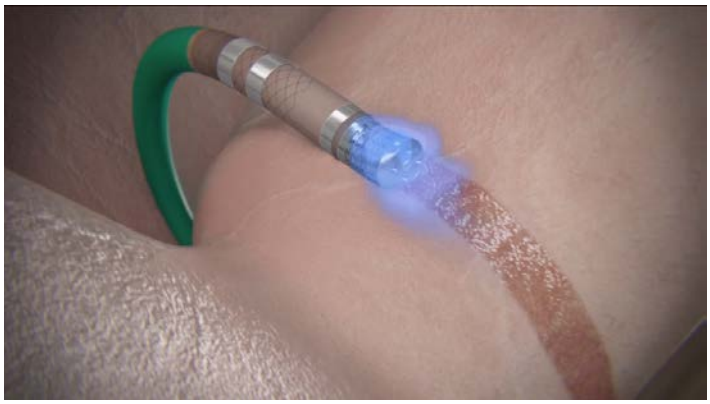

***Figure 6**: Artist representation of irrigated ablation catheter on atrial tissue. The ablated tissue is represented in dark pink, the atrial tissue is light pink, and the blue represents the irrigation fluid being applied during the ablation process (Figure from Biosense Webster)*[22]

This is done in order to minimize the unintended ablation of tissue that is not causing the aberrant electrical pathway in the tissue and serves to "focus" ablation energy to the intended area as in Figure 6.

An alternative to RF ablation is the use of cold temperature to create lesions in tissue.[1] Cryoablation uses a balloon catheter inserted into a blood vessel, usually in the femoral vein, and then threads it though the body until it reaches the heart. This narrow tube has an inflatable balloon on the distal end that engages the pulmonary vein. Using imaging techniques, the doctor is able to guide the catheter to the heart. Once the balloon is in position at the tissue of interest, refrigerated fluid flows through the catheter to create the lesions in the tissue that eliminate the aberrant heart rhythm.[1] The cryoballoon allows for cryothermal application over a larger surface area than RF ablation procedures. Catheter manipulation and correct positioning of the ablation catheter remain key ingredients for a successful procedure both in terms of effectiveness and safety. Failure to fully provide therapy to the targeted tissue during cryoballoon lesion delivery is usually due to incomplete

contact and leads to a lower chance of targeted tissue isolation and a higher risk of recurrence of aberrant heart rhythm.[19]

2.2 Innovation

Novel, physically pliable silicon-based electronics developed in John Rogers' laboratory offer the ability to easily conform electrical circuits to the dynamic surface of a beating hearts.[29-32] Sub-millimeter and sub-millisecond resolution electrical recordings cardiac tissue can be obtained using a matrix of transistors, (Figure 7).

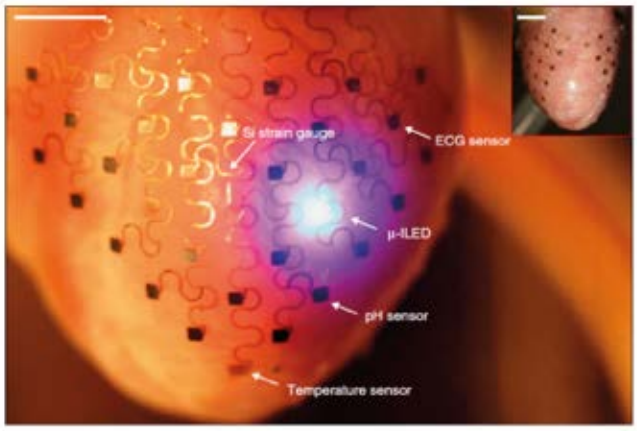

***Figure 7**: Conformal electronics adhered to surface or rabbit heart with various sensors (Figure from Kim et al.)[29]*

The recording function of these electrodes has been previously evaluated on porcine, rat, and rabbit hearts in proof of concept sensing and pacing studies tested on a small strip of left ventricle. The conformal electronics used in these studies were based on passive resistive electrode technology, which requires contact with the tissue, is prone to current leak and the acquired signals can only be processed on a separate system.

2.2.1 Utilization in Balloon Catheter

The use of balloon catheters imbued with multiple sensors has been characterized previously in literature and has been shown to work in animal models.[31] The balloon-catheter device is attractive for endocardial procedures such as AVNRT ablation therapy because it enables minimally invasive insertion into lumens or other organs of the body through small incisions, because of the miniaturized, cylindrical form of its deflated state, and it can be inflated, to match requirements on size and shape for its interaction with the endocardial tissue. The main disadvantage is that conventional balloons offer minimal utility, because of their uniform sheets of electronically and optically inactive materials, such as polyurethane or silicone.[31] Commercially available catheters (8–18 Fr diameter) serve as the delivery mechanisms and the general template for the device.[31] Components that integrate with the balloons are formed on semiconductor wafers using adapted versions of planar processing techniques and methods of transfer printing reported elsewhere.[33] Wrapping the collections of interconnected devices on the balloon in its deflated state creates the planar surface with the active components imbued on top.[34] Encapsulating layers serve as moisture barriers to enable the entire system to operate when completely immersed in bio-fluids. These devices sense physiological signals and stimulate tissue. They are connected and powered through a thin ribbon cable based on an anisotropic conductive film that bonds to the base of the shaft that connects to the balloon, and wraps along the length of the flexible tubing of the catheter. These procedures add functionality to balloons (figure 8) without significantly altering their mechanical properties or the levels of expansion that they

can accommodate. The mesh layouts can tolerate tensile strains of up to 200% without fracture, owing to optimized configurations guided by quantitative mechanics modelling.

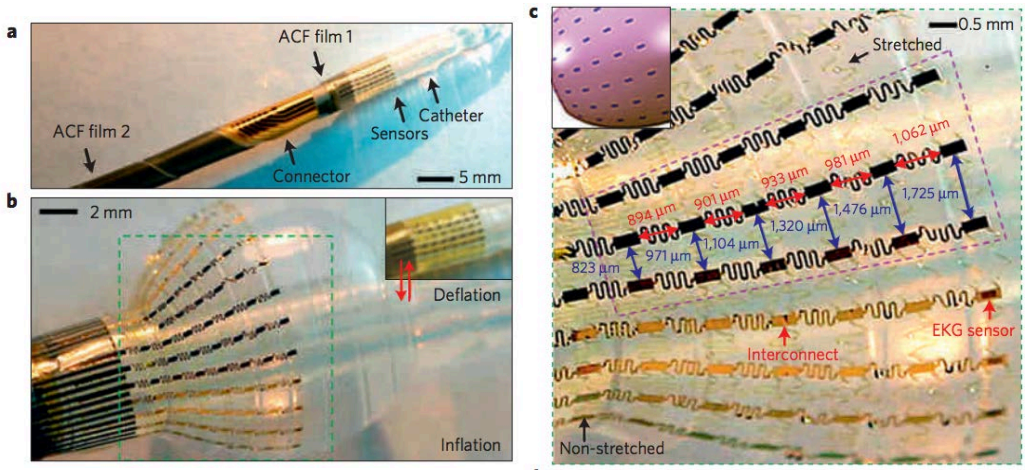

***Figure 8a**, A stretchable, interconnected passive network mesh integrated on a balloon catheter (deflated) showing the overall construction, including connectors and ACF metal traces on the proximal side of the balloon and its wrapping configuration along the length of the catheter shaft. b, Optical image of the balloon inflated by ~130% relative to its deflated state (inset). c, Magnified view of non-coplanar serpentine interconnects on the balloon in its inflated state. This region corresponds to the area defined by the green dotted line in b. The spacing between the sensors and the configurations of the serpentine interconnects compare well with simulation results. (Figure from Kim et al.)*[31]

2.2.2 Chiplet Technology for Mapping

The next generation conformal electronics technology called the Chiplets, utilizes the flexible and stretchable electronics membrane and is now populated with hundreds of self-contained microcircuit assemblies called “chiplets” comprised of integrated actuators, sensors, amplifiers, and multiplexers. These developments have the promise of allowing for the creation of devices with larger scale and higher density of sensors than current technologies with which to map the aberrant cardiac tissue and can be readily achieved in a way that leverages advanced processing techniques. These would allow for coverage across entire sections of cardiac tissue by affixing layers of electronics to the flexible board. There are no fundamental

hurdles, for example, in achieving systems with thousands or even hundreds of thousands of electrodes for mapping electronic signals of the cardiac tissue. Autocorrelation methods can be used to identify the node spacing that will maximize acquisition of electrophysiological data while reducing unnecessary redundancy. Coverage across endocardium tissue can occur by integrating the electronics onto or into the surface of a balloon catheter. Energy delivery capabilities for both pacing and ablation could stem from developing high definition capacitively coupled stimulators. The new innovations in the field allow large area, conformal electrodes suitable for sensing cardiac electrical activity, and delivering cardiac electrical stimulation has the potential to enable clinically safe systems capable of diagnosing and treating patients with life threatening arrhythmias in real time.[29, 35-36]

The technology by John Roger's group is the first to incorporate all of the key features needed for use in high-speed, high-resolution cardiac electrophysiology.[37] First, it facilitates large area formats with integrated active electronics for multiplexing and signal amplification on a per-channel level. It utilizes thin, flexible device mechanics for integration and high-fidelity measurement on the curved, moving surfaces of the heart. The cumulative levels of leakage current to the surrounding tissue that remain well below 1 μA for safe operation.[37] It has long-lived, thin, bendable bio-fluid barriers as, hermetic sealing of the underlying electronics for stable, reliable function. And biocompatible interfaces for long-term use, without either direct or indirect contact to traditional electronic materials. Prototype designs used in previous testing has consisted of 396 multiplexed capacitive sensors (18 columns, 22 rows), each with dimensions of 500 ×500 μm, as

shown in Figure 9, distributed uniformly over a total area of 9 × 11 mm for a density of 4 sensors/mm^2.[37] Each sensor consists of two underlying Si NM transistors, one of which connects to a metal pad from its gate electrode (Figure 9). A layer of thermally grown silicon dioxide covers the entire top surface of the system (Figure 9). This thin thermal SiO2 layer as the dielectric for capacitive coupling of adjacent tissue to the semiconducting channels of the associated Si NM transistors, and as a barrier layer that prevents penetration of bio-fluids to the underlying metal electrode and associated active electronics. The total thickness of the chiplet is 38 μm. This fabrication process is capable of scaling up to the largest silicon wafers available which is currently 450 mm diameter.[37]

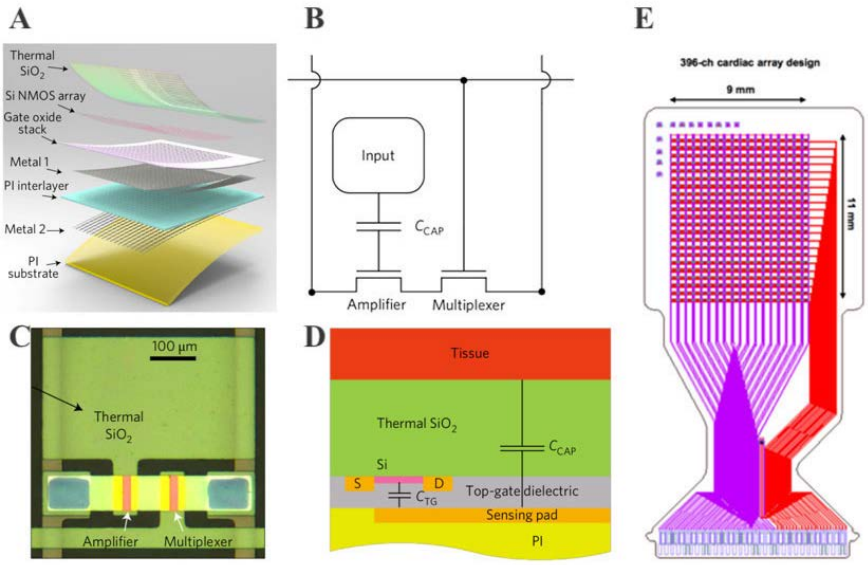

***Figure 9A**: an exploded-view schematic highlighting the key functional layers. B: circuit diagram for a node in this capacitively coupled array, with annotations for each component. C: optical microscope image of the cell. D: schematic of the circuit cross-section E: Schematic illustration of an 18×22 array of active multiplexed channels (Figure from Fang et al.)*[37]

2.2.3 Ablation and Pacing Electrodes

Exposed electrode pads provide electrical contact directly to the tissue for the purpose of RF ablation. Variations in temperature laterally along the surface of the tissue and into its depth characterize the critical aspects of lesions formed by this ablation process. When combined with quantitative modelling of the ablation process and thermal diffusion, these measurements provide both types of information. To this end, Kim et al. developed nonlinear models for characterizing electrical and thermal transport, and validated them through comparisons to measurements of in-plane temperature distributions created using a single RF ablation electrode (inset in Figure 10a) against a piece of tissue from a chicken breast (□15 cm×15 cm).[31] A representative measurement appears in Figure 10a, with an ablation electrode (290 × 560 μm), and an applied voltage oscillating between +9 and −9 V in a 450 kHz sinusoidal waveform. Heat released during ablation results from current that flows between the small active electrode and the ground electrode. At steady state, a voltage of 6.1V gives a maximum temperature of 70 ◦C and an in-plane distribution (Figure 10b) that are consistent with experimental observations. Figure 10c shows the temperature distributions along the radial and thickness directions, which can be used to estimate the lesion size and depth. For a representative temperature 50°C, the lesion size (diameter) is 1.6 mm, and lesion depth is 0.8 mm (Figure 10d).[31]

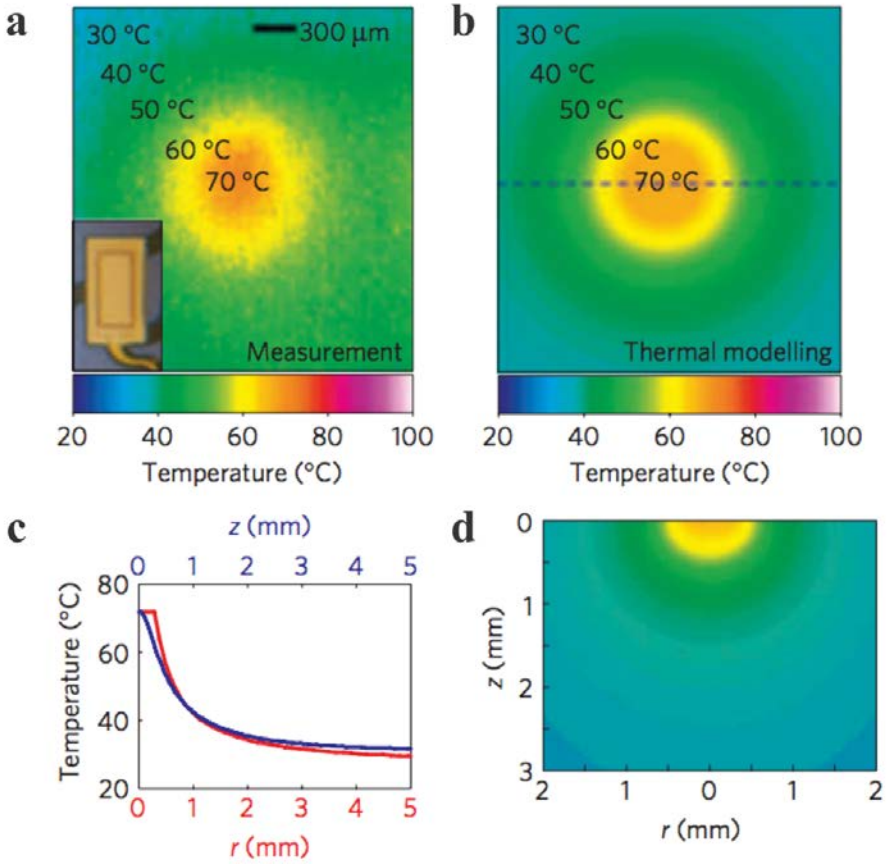

***Figure 10A**: Infrared-camera image of the distribution of temperature in tissue created by activation of an RF ablation electrode (inset). The highest measured temperatures (~70 ◦C) coincide with the location of the electrode. b: Temperature distributions determined by coupled thermal and electrical modelling of the ablation process. c: Modelling results for thermal distributions along the radial (r) and transverse (normal; z) directions. d: Distributions in both radial and transverse directions for the cross-sectional plane indicated by the blue dashed line in b. (Figure from Kim et al.)*[31]

The same electrodes that are used for ablation can also be used as pacing electrodes for delivering lower energy and lower frequency current to the heart for the purposes of verifying that the ablation has been successfully delivered.[31] The electrical specifications of an electrode to be used for pacing require that the applied voltage to tissue be limited to 5V at a frequency of up to 300Hz. At these low thresholds of pulse input to the catheter, the electrodes in contact with the tissue would be functioning as traditional pacing electrodes and not as ablation devices.[31]

2.2.4 In-vitro Electrical Performance

The performance of the capacitively coupled active sensing nodes is stable across a broad time dynamic range.[37] Figure 11a shows high-gain, low-noise measurements for input signal frequencies between 0.1 and 100Hz. The power spectral density (PSD) of the output signal, computed from the Fourier transform of the auto-correlation function, describes its frequency behavior. Figure 11c displays a 396-channel sensing system with mean noise as low as ~55 μV, signal-to-noise ratio (SNR) over 42 dB, and uniformity across the entire device. Statistics on the test transistor threshold voltage, mobility, array yield and average gain from different devices show very small sample-to-sample and batch-to-batch variations (Figure 11d, e).[37]

Mechanical bending tests and in vitro soak tests demonstrate the flexibility and mechanical robustness of the system (Figure 11, g). For 5 mm bending radii, finite element analysis indicates that the strain induced in the Si and top SiO2 layers are less than 0.025%, far below their fracture limits (~1%). The device performance remains unchanged in the bent state and does not vary after bending to a radius of 5 mm for up to 10,000 cycles (Figure 11h). Infrared imaging testing also reveals that there is no apparent increase in temperature associated with operation of the device. The system also demonstrates nominal operation while immersed in saline solution and bio-fluids, as a result of the thermal SiO2 encapsulation.[37] The soak test, where PBS solution simulates the cardiac bio-fluid is depicted in Figure 11g. The device was tested via the application of a 3 V DC between the sensing system and a Pt reference electrode at a temperature of 37 °C. The leakage current is lower than

10−9 A/cm^2 for at least 120 days submersion (Figure 11i). Figure 11j shows the frequency response to a 10 Hz sine-wave input, before and after the bending and soaking experiments.

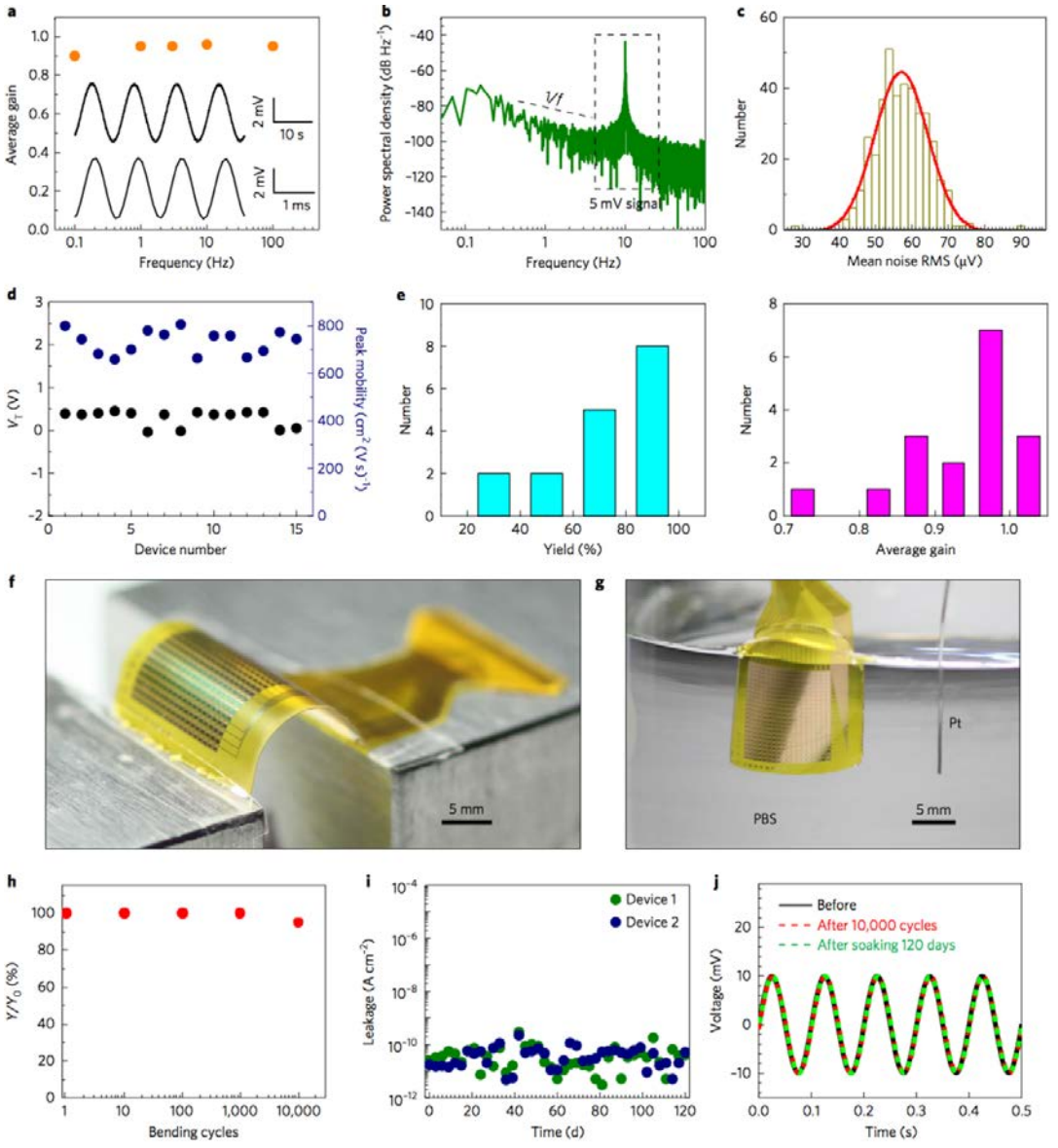

Figure 11 *In vitro assessment of electrical performance a, Average gain of a representative capacitively coupled transistor as a function of the input frequency from 0.1 to 100 Hz. The inset shows the responses from this sensor node at 0.1 Hz (top) and 100 Hz (bottom), after band-pass filtering (0.05–568 Hz). b, Power spectral density of a 5 mV AC. signal at 10 Hz measured at a representative node, showing a typical 1/f relationship at low frequency. The input was a sine wave of 5 mV at 10 Hz. c, Histograms of noise (with Gaussian fitting) measured from all 396 nodes of the device in Figure c. d, Statistics of the threshold voltage (VT) and peak effective mobility (μeff) of test transistors from 15 different arrays. e, Statistics of yield (left) and gain (right) of 17 capacitively coupled, active sensing 18 × 22 electrode arrays. f, An image of a device during a mechanical bending test. g, An*

image of a device completely immersed in a saline solution, during a soak test. PBS, phosphate-buffered solution. h, Yield (Y, defined as the number of working nodes divided by the total number of nodes) as a function of cycles of bending to a 5 mm bend radius, showing minimal changes up to 10,000 cycles. i, Electrical leakage current of 2 devices during soak testing. Minimal leakage appears over a period of 120 days at 37 °C. j, The response of a representative node to a sine-wave input (at 10 Hz) before, after 10,000 cycles of bending and after saline immersion for 120 days (Figure from Fang et al.)[37]

2.2.5 Animal Model Performance

Experiments that validate the function were performed by recording unipolar voltage signals from all 396 nodes on multiple ex vivo Langendorff perfused rabbit hearts.[38] Figure 12a shows a system placed on the anterior aspect of the heart with equal overlap on the right and left ventricles. The device conforms to the curvilinear surface of the heart. Capillary forces associated with the moist cardiac surface can fixate the device in place, however, the use of a thin polyvinyl chloride (PVC) film wrapped around the heart further enhances the robustness of the mechanical coupling. A representative single-node voltage trace during sinus rhythm is shown in Figure 12b. Clear components, similar to the P wave, QRS complex and T wave in clinical electrocardiogram (ECG) recordings, are apparent and the low noise levels are consistent with the in vitro results. Attaching the device on the heart does not interfere with the heart's rhythm, based on experimental observations. High-definition electrophysiology mapping results from plotting the signals from all 396 nodes as a function of time. Spatial voltage maps of all nodes at four sequential time points are show in in Figure 12c, corresponding to phases 4 to 1 in the cardiac action potential where dashed lines in Figure 12b illustrate the time window in which Figure 12c is taken. The wave of cardiac activation approaches the center of the anterior aspect of the heart from both the left and right sides, which matches well the physical location of the device. The extracted conduction velocities (0.9506 ± 0.3340

mm ms−1) are close to values from optical data (0.8124 ± 0.3438 mm ms−1) taken concurrently.

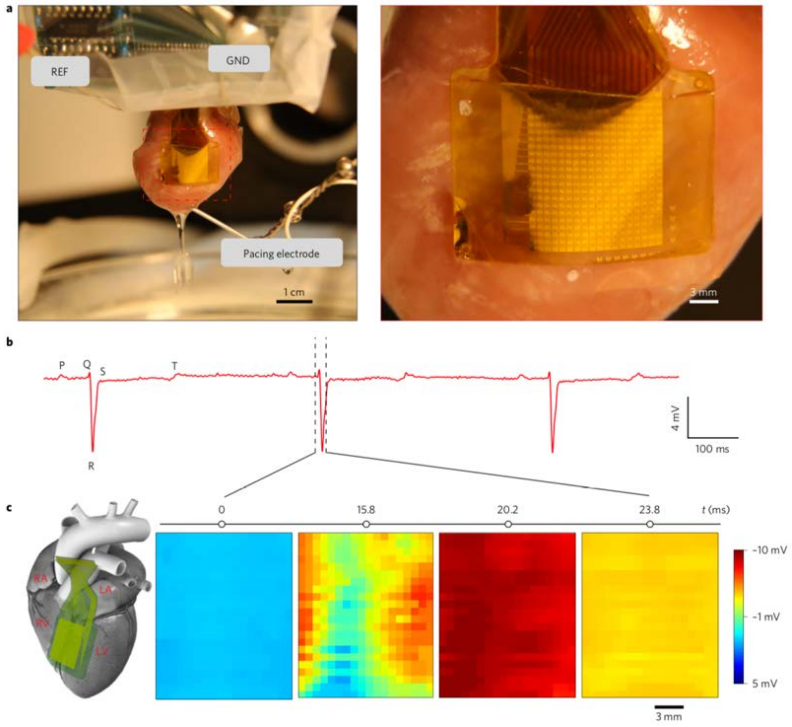

Figure 12: *High-density cardiac electrophysiological mapping on ex vivo rabbit heart models. a, A photograph of a flexible capacitively coupled sensing electronic system on a Langendorff-perfused rabbit heart (left). REF and GND represent the reference and ground electrodes, respectively. The magnified view (right) shows conformal contact of the device to the cardiac tissue, through the action of surface tension. b, Representative single-voltage trace from the electrode array without external pacing. Signatures related to the P, Q, R, S and T waves in ECG traces can be identified from the recordings. c, Representative voltage data for all electrodes at four time points (indicated in b), showing normal cardiac wave-front propagation. The progress of the cardiac wave is consistent with the physical location of the array on heart, as illustrated in the diagram on the left (RA, LA, RV and LV: right atrium, left atrium, right ventricle and left ventricle, respectively). (Figure from Fang et al.)*[37]

Chapter 3: Proposal and Methods

3.0 Proposal

The novel materials and electronics technology allows for the development of novel device for use in clinical practice. This device would be able to address a major shortcoming of current devices by integrating the mapping, pacing and ablation phases of AVNRT ablation procedures into one device. The high-density mapping capabilities of such a device would more quickly and precisely find the area of the atrium that requires ablation. Using the same device, and without moving that device, the ablation electrodes spread throughout the surface could be selectively activated to deliver the RF energy needed for tissue ablation. Again using the same device, and again without moving the device, the pacing electrodes spread throughout the surface of the device would deliver an arrhythmic pacing energy to verify that the AVNRT pathway has been sufficiently ablated.

Additionally, the device could include a distal tip for the purpose of anchoring the device to an ostium within the endocardium such as the CS so that motion due to cardiac contraction is minimized and the device can maintain contact with the endocardial wall.

Incorporating the necessary electrical components onto the flexible PCB material of the balloon that would provide RF therapy from the same balloon catheter would enable the development of a device capable of delivering appropriately targeted ablation energy without the need to position other catheters into therapeutic position. Such a device would provide all the functions of various catheters that are used in the mapping/pacing/treatment of RF ablation procedures in one multipurpose device that can “automatically” diagnose and treat tissue.

3.1 Design Requirements

The primary design requirement and ultimately the purpose of this thesis is to create a single device that map, ablate, and pace the atrium for patients with AVNRT. It must be large enough so that the active components of the device are in contact with the region of interest. The device must be able to correlate a mapped section of aberrant tissue to ablation electrodes for targeting that tissue. The device must be stable during use inside a beating heart. The density of the electrodes for mapping should be adequate for locating aberrant tissue. The density of ablation electrodes should be sufficient so that the ablated tissue around a single electrode can overlap/meet the tissue that would be ablated by an adjacent electrode. The pacing electrodes must be present in the ToK so that the AVNRT pathway is triggered after ablation to ensure successful treatment. The device must be able to be delivered to the right atrium as well as retracted after use. Each of these design requirements must be evaluated to fulfil a clinical or engineering specification so that the specification of the device meets the requirements.

3.2 Characterize ToK Anatomical differences

The first task in the design of the device is to determine the functional anatomical area that will be of interest in the patient atrium to drive the dimension specifications of a device. Areas of interest in the heart were isolated from radiology scans of patients to determine the topographical and physiological constraints that must be addressed for device design. The clinical images from the George Washington University Radiology Clinic were gathered from patients undergoing chest MRI

scans for the any purposes. The scans were collected and had any personally identifiable information removed, including, name, age, gender, and condition of health. The MRI images were provided in DICOM format in axial, coronal, and sagittal views. Using the open-source Seg3D segmentation program, the images were filtered and segmented.

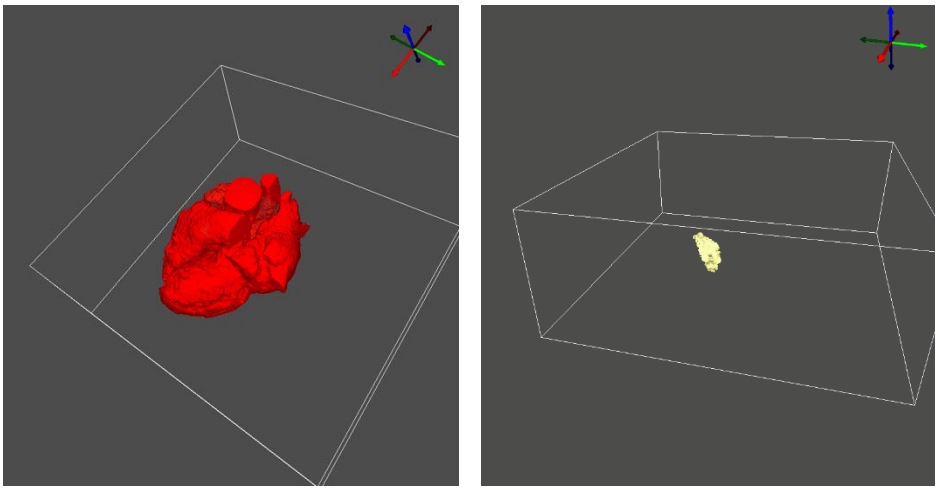

Figure 13 *Left: Heart Segmentation in Seg3D software; Right: Triangle of Koch Segmentation*

MRI Scans were provided data on 21 total patient scans. The dimensions of the segmented ToK was evaluated using Osirix Lite software and the surface area of ToK calculated. The results of the nine measurements show an average area of 319mm2 with a standard deviation of 88mm2 and a measurement range of 182-452mm2. The results of the measurements taken of the heart segmentations were compared to findings in literature. Zhivadinovic et al. measured the dimensions of the Triangle of Koch in 50 adult patients post-autopsy and found the average ToK area to be 261mm2 with a standard deviation of 52mm2 and a range of 160-375mm2.[39] Additionally, Yamagushi et al. used a NavX mapping system to map the physiology of 42 adult patients undergoing slow pathway ablation procedure. The

study found that the Average area of the ToK was 296mm2 with a standard deviation of 85mm2 and a range of 132-490mm2.[40] The results of the measurements are summarized in Figure 14 below. Comparison to literature showed statistical agreement by 1-Sample t-test agreement between the measured values and previously reported studies into the anatomical variations of the ToK.

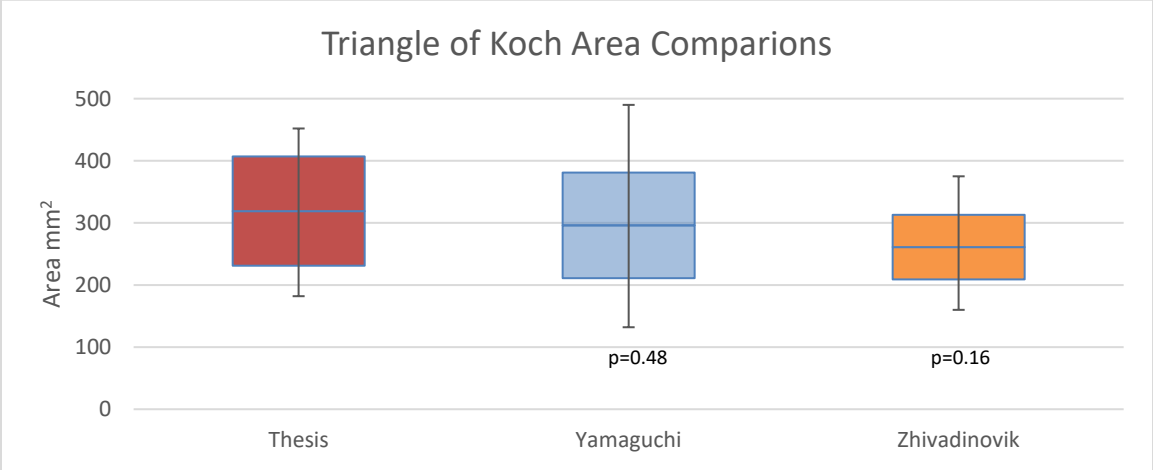

***Figure 14**: Box denotes standard deviation from midline mean. Lines denote range of data. P-Value is 1-Sample t-test of measured data compared to summary data from literature.*

Yamaguchi also classified the ToK areas into three distinct small, normal, and large Koch sizes based on the observed sizes. The averages of the ToK areas in each size was calculated and the standard deviations reported. The classifications used by Yamaguchi are detailed in Figure 15.

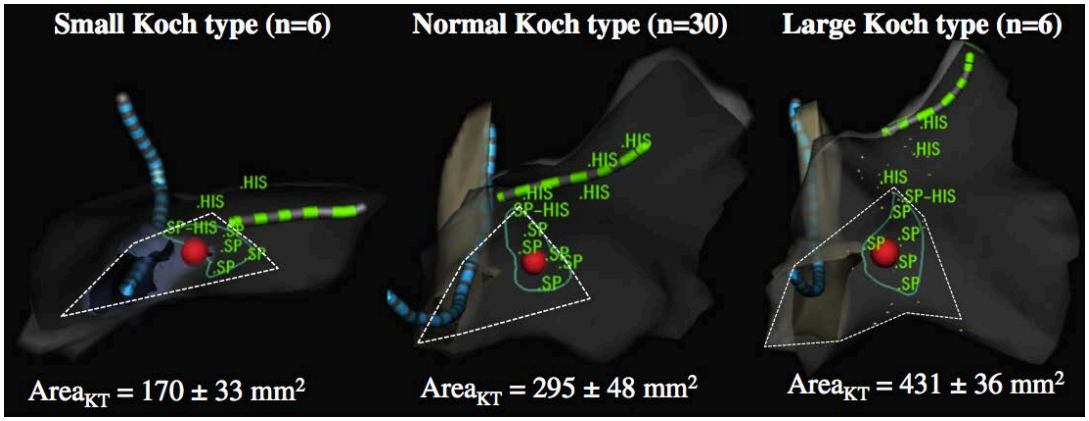

Figure 15: *Classification of ToK size measurements (Figure from Yamaguchi et al.)*[40]

The measurements show that three size areas for the ToK exist in a given population. The measurement data conducted on the heart segments and acquired from literature agree that that the ToK area is approximately 250-300mm2 on average but can vary significantly to almost half that area measurement or double that area measurement. A device design capable of serving the largest ToK area size of ~500mm2 would represent a normal size device with alternate small devices utilized in patients with a ToK area measurement of less than 200mm2. Although the area of the ToK does not need to be precisely known prior to the patient catheterization procedure, an approximation of the size of the ToK and the use of an appropriately sized device would prove useful if empirical measurements show that a smaller device has better contact in patients with smaller areas of the ToK. This thesis will focus on the design of a device used in the largest observed ToK measurement of 500mm2, though creation of a smaller device would be largely trivial and involve scaling the dimensions of the flexible circuit board imbedded with electronics. The use of a large device allows for freedom to partially inflate the

balloon catheter during a procedure if the ToK is smaller than the dimensions of a fully deployed balloon.

3.2.1 Quantitative Analysis of Dimensions

The preferred embodiment of the device designed to be applied to the ToK is one of a balloon catheter that can be inflated in the right atrium and contacted to the endocardial tissue that comprises the Triangle of Koch. Measurements of the ToK done for this thesis show that the longest distance from one point of the TOK to another is along the TV with the longest measured length being 43mm. If the distal tip of the catheter is inserted into the CS to provide stability, the inflated balloon would need to reach from the center of the CS to the furthest end of the ToK 43mm away.

Flattening the catheter would significantly reduce the volume it occupies within the atrium when inflated, while also serving to maximize the distal surface area that comes into contact with tissue. This can be done by utilizing a retractable distal section of the catheter that decreases the distance between the ends of the balloon and reduces the sphericity of the balloon so as to make an oblate spheroid which resembles of a “puck” or “pancake” shape as shown in Figure 16. In doing so, it can significantly reduce the amount of material needed to be deployed within the atrium while maintaining the same coverage of the ToK and mapping and treatment capabilities. The longest measured length from the coronary sinus to the Bundle of His was 43mm. Using the reference distance of 43mm as a radius for what a flattened balloon side (this is effectively a 2D circle

pressed to the tissue) must be to cover the area from the CS where the catheter tip would be anchored, to the end of the ToK,

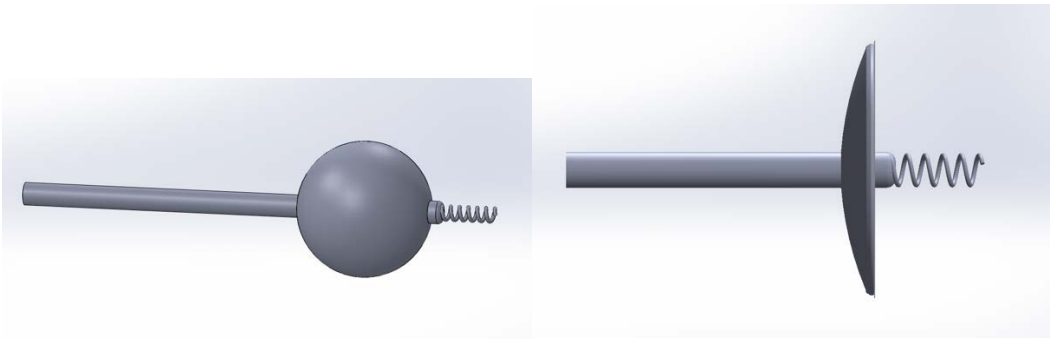

***Figure 16**: Left: Inflated balloon catheter model Right: Profile view of Flattened-inflated balloon catheter ready to make contact with endocardium.*

Maintaining an oblate spheroid structure by inflating the balloon and compressing the ends together gives the balloon catheter structural rigidity in order to apply contact to the endocardial wall without the use of rigid components that may be dangerous to introduce into the atrium. Additionally, it allows for the device to meet the dimensional requirements of a device that can cover the entire ToK of a patient with the largest observed area. The oblate spheroid design also allows for the ability to inflate the device to a lesser extent if the patient ToK is smaller and the fully expanded distal half of the balloon is not required to be pressed against the ToK.

3.3 Electrode Layout

The catheter would only need to have sensors placed on the distal hemisphere for contact with endocardial tissue when inserted into the right atrium. This means that the proximal half of the balloon can be composed of more traditional and flexible materials such as polyurethane to reduce complexity of the device. Additionally, the longest length of any side of the ToK measured was 43mm.

Therefore, the balloon would only need to have electronics placed on a 60˚ arc with a radius of 43mm with the rest of the balloon catheter being comprised of traditional materials.

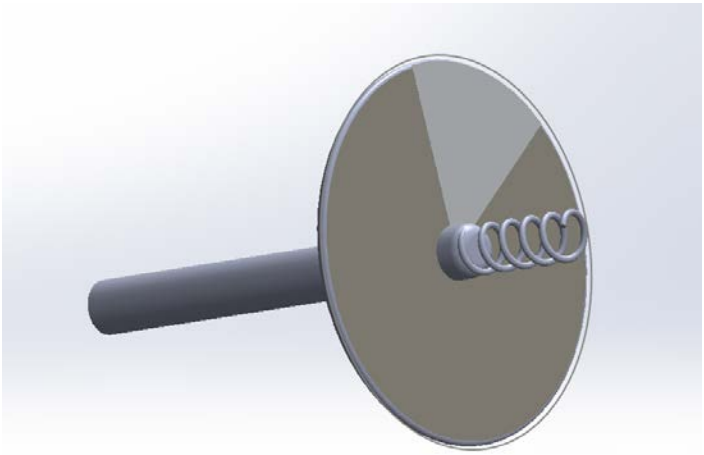

Figure 17: *Balloon catheter model in fully deployed oblate spheroid configuration. Light Gray section shows active electronics region of balloon to be pressed to ToK*

As previously stated, the technology is readily transferable to a 450mm diameter wafer design. Therefore, a configuration with the distal end of the device imbued with the novel conformal electronics could be implemented for an 86mm diameter wafer for manufacturing which is then divided into 6 segments for utilization in catheters.

The design of the conformal electronics allows the electrode layout to become less important than in previous devices that incorporated multiple sensors on the same catheter due to the density of sensors that can be placed throughout the active surface of the device. The distal half of the balloon catheter in the oblate spheroid configuration is 5808mm2 with 113mm2 in the center unavailable because of the lumen of the catheter. The active area of electronics is a 60˚ arc

with radius 43mm and a surface area of 968mm^2 a region of space with 5mm radius at the base of the arc is unavailable which the lumen of the catheter must pass through. This means that 916mm^2 of the balloon is available for placement of electronics.

As previously discussed, each ablation electrode is 290x560µm and can ablate a region of tissue with 1.6mm diameter. The same electrodes can also be used to deliver pacing energy to the endocardium. In order to realize the design requirement that the device must be able to ablate any point or set of points along the slow pathway, the ablation electrodes must be no further than 1.6mm apart. This distance also ensures that ablation can occur along a continuous vector of electrodes if a large area of tissue or a linear area of tissue needs to be ablated. Ablation electrodes were present on alternating rows of electronics. For the purposes of this design, the wiring of the electrodes will be done in such a way that it is routed on the opposite side of the PCB, and through the lumen of the device. The 5mm lumen of the catheter has 78.5mm2 of cross-sectional to route the necessary electronics through. Though, additional information about the wiring and dimensional requirements are necessary to create a means by which to deliver power to the sensors and receive information from them. This is especially important as the lumen will incorporate a retractable support rod that extends distally to maintain the other end of the balloon and the distal tip of the balloon as well as a means of delivering fluid to the balloon for inflation.

Figure 18: *Left, Detailed angled view of mapping electrodes with ablation and pacing electrodes interspersed electrodes showing height. Right, Full arrangement of electrodes on balloon distal half.*

The active electronics area is comprised of repeating sections of electronics each 15˚ in angle together to create the 60˚ arc that will be used to sense and ablate within the atrium. Each section has sensor and ablation electrodes arranged in linear rows for ordered packing. For some rows, it was necessary to enter two adjacent mapping sensors so that the spacing allowed for an ablation electrode to be placed at the end of the row. The reason for the ablation electrodes to be placed on the end of the rows is to ensure that the edges of the active electronics assembly are able to ablate tissue that may be located at the extreme edges of the device. Placing ablation electrodes on the ends of rows ensured that no ablation electrode was ever more than 1.6mm apart from the adjacent one. Figure 18 shows a diagram of chiplet electrodes and sensors dispersed in an arrangement allowing for ablation electrodes (seen as longer, narrower bodies) never more than 1.6mm apart to ensure that any area of the balloon can have energy delivered to it at any time. The final arrangement of electronics included 944 ablation and pacing electrodes and 2496 mapping sensors.

3.4 Deployment Mechanism

When the device is being deployed, the balloon must be folded within the catheter assembly and inflated within the atrium to the desired size. Folding is a commonly used manufacturing step for balloon catheters and commercially available equipment would be able to be ordered for any design specification.[41] However, the flexibility of the chiplets is limited to bending along an arc with a radius of 5mm. Any catheter pleating and folding design would require the balloon surface to be folded about an arc with radius of 0.02mm. Therefore, the active electronics on the balloon would have to be wrapped around the lumen of the catheter with the balloon folded to fit within the lumen of the catheter. The largest catheter in clinical practice is 18Fr or 6mm diameter. The chiplets on the active section of the balloon are 43mm across at their longest point. That means that the chiplets must be wrapped around a 5mm diameter catheter lumen with circumference 15.7mm three times to leaving 1mm of space within the catheter to leave space for packing of catheter balloon around the wrapped chiplet electronics.

The chiplets at their widest point are 38 μm in thickness. Adherence on a 1.4 μm thick polyurethane balloon typically used in other balloon catheters would increase the total thickness of the balloon to 39.4 μm.[42]

This design has one significant drawback that must be addressed. The chiplet arrays have been tested to bend about an arc with a 5mm radius and have shown that the strain induced in the Si and top SiO2 layers are less than 0.025%, far below their fracture limits (~1%). The device performance remains unchanged in the bent state

and does not vary after bending to a radius of 5 mm. However, the design about an 18 Fr catheter necessitates that the chiplets be tested to bend around a radius of 2.5mm. Though the testing showed that the 5mm radius bending tests were 40x below the chiplets fracture limits, the chiplets must still be validated to perform at greater strains. **3.5 Anchoring Mechanism**

In order to minimize the effects of motion caused by the heart beating on the balloon catheter signal acquisition and energy deliver, it is necessary to anchor the distal tip of the catheter into the coronary sinus of the heart so that the catheter moves with the heart. Insertion of the distal tip into the CS to stabilize the catheter must be done in a way so that the catheter does not occlude the flow of blood from the CS. A helical protrusion from the distal tip of the catheter would be able to provide the necessary stability while allowing for the flow of blood from the CS into the RA. The catheter could also be anchored in place by the use of pressure from the catheter turning within the chamber of the hear as it emerges from the Inferior Vena Cava after the catheterization from the femoral vein. The application of two pressure points on the catheter would serve to minimize motion of the electronics in contact with the ToK.

3.6 Design Specifications

The primary design requirement to create a single device that map, ablate, and pace the atrium for patients with AVNRT is met by the use of the chiplet electronics for mapping of the endocardium and ablation and pacing electrodes for the delivery of energy to the tissue. It must be 43mm in radius when shaped into an oblong spheroid so that the active components of the device are in

contact with the region of interest and so that the entire ToK is accounted for in patients. The device must be able to correlate a mapped section of aberrant tissue to ablation electrodes for targeting that tissue via the use of multiplexed electrodes. The is device stable during use inside a beating heart by anchoring the distal tip of the catheter into the coronary sinus. The density of the electrodes for mapping is adequate for locating aberrant tissue and via the inclusion of 2492 electrodes on the balloon surface. The density of 944 ablation and pacing electrodes is sufficient enough so that the ablated tissue around a single electrode can overlap/meet the tissue that would be ablated by an adjacent electrode by being designed to never be further than 1.6mm apart; the same as the measure of tissue which the electrodes have been tested to ablate. The device must be able to be delivered to the right atrium by the use of pleating on the balloon for compact deployment. Each of the design requirements has been evaluated to fulfil a clinical or engineering specification to meet the device requirements.

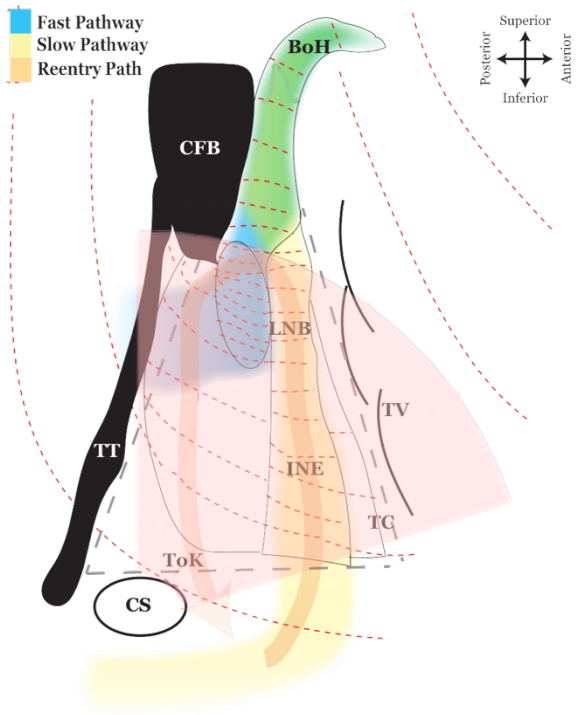

Figure 19: *Device active electrode area overlaid on anatomy of ToK showing complete coverage of areas of interest. (Figure modified from Sharon A. George, Department of Biomedical Engineering, The George Washington University)*

3.7 Comparison of Workflow

A comparison of the workflow currently practiced for the ablation procedure in AVNRT is to the proposed workflow that an automated balloon catheter would enable is provided in Figure 18.

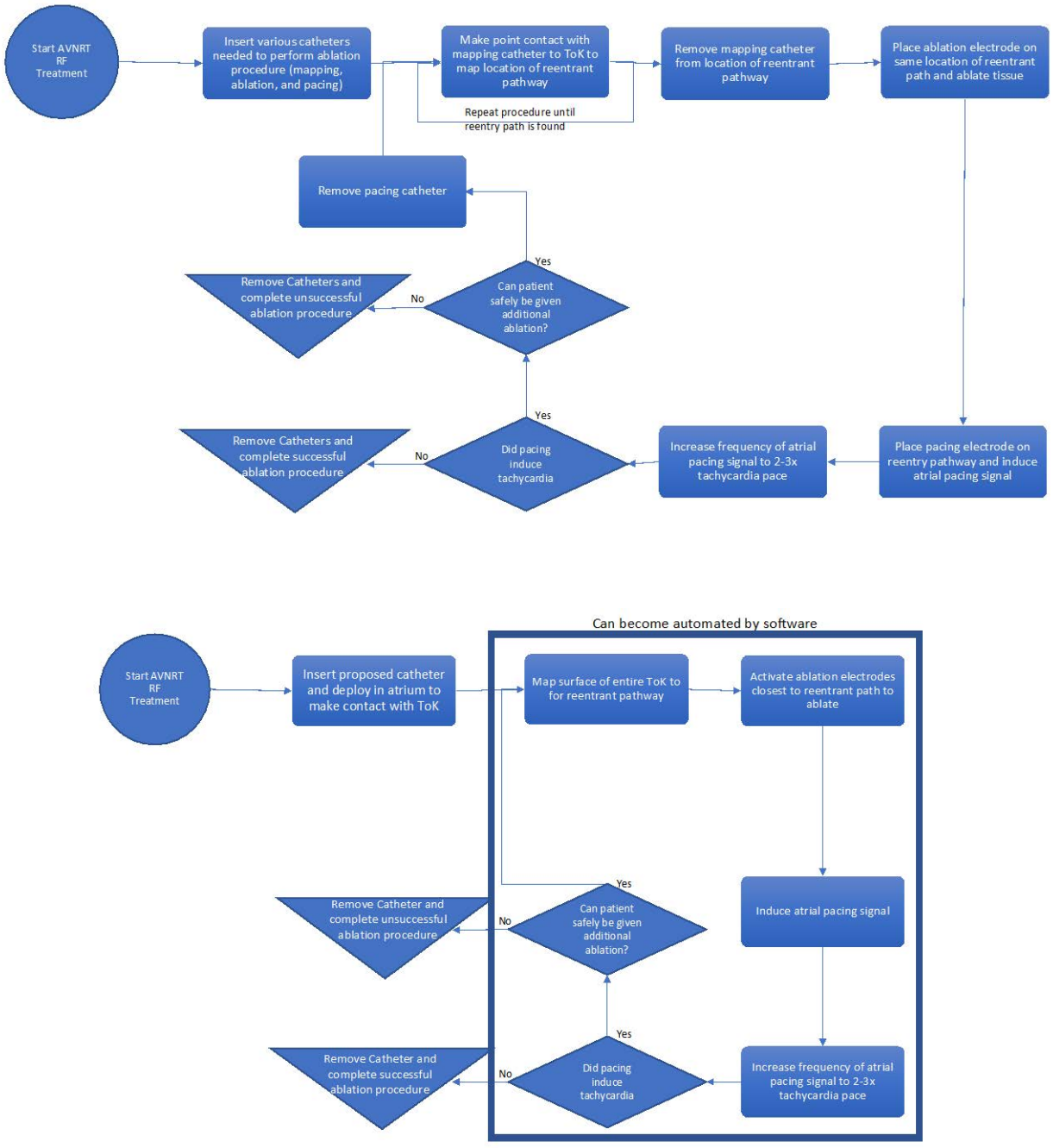

Figure 20: *A comparison of the AVNRT ablation procedure work flow as is current practiced (top) compared to a workflow using the proposed device (bottom)*

3.8 Patent Generation

In order to proceed with the design of the inflatable balloon design, a provisional design patent was published for the purpose of securing the intellectual property

of such a device. The patent was structured to encompass three generations of devices with each subsequent device being capable of more complex functionality.

The first-generation device is a flexible balloon circuit board design with high resolution, multi-function, conformal electronics device generally consisting of flexible and stretchable, high-density (thousands) electrode array, integrated with existing catheter-based technology (e.g., balloon catheter) for mapping of and corresponding localization of the arrhythmia source. The active sensing electrode array can acquire diagnostic information including electrical (e.g., electrograms), mechanical (e.g., strain measurements), impedance (e.g., resistance), metabolic (e.g., pH measurement) from the underlying heart tissue surface in contact. In the preferred embodiments, the electrode array may be designed to be of various sizes and shapes to conform to the targeted cardiac tissue architecture (e.g. atrial, ventricle, right ventricular outflow tract, coronary sinus etc.,) corresponding to the specific type cardiac arrhythmia.

The second-generation device combines the ability of the first generation to precisely locate the source of arrhythmia with the ability to deliver therapy from the same electrode array. This is achieved through the use of capacitive sensing electrode array that can not only monitor but also deliver electrical stimulation. The electrode array can acquire diagnostic information including electrical (e.g., electrograms), mechanical (e.g., strain measurements), impedance (e.g., resistance), metabolic (e.g., pH measurement) from the underlying heart tissue surface in contact as well deliver electrical stimulated to the precise location

diagnosed as the source of arrhythmia. In the preferred embodiments, the electrode array may be designed to be of various sizes and shapes to conform to the targeted cardiac tissue architecture (e.g. atrial, ventricle, right ventricular outflow tract, coronary sinus etc.,) corresponding to the specific type cardiac arrhythmia.

The third generation combines the ability of the first generation to precisely locate the source of arrhythmia, and the second generation to deliver therapy from the same electrode array with the new ability to be implantable into the patient. The electrode array can acquire diagnostic information including electrical (e.g., electrograms), mechanical (e.g., strain measurements), impedance (e.g., resistance), metabolic (e.g., pH measurement) from the underlying heart tissue surface in contact as well deliver electrical stimulated to the precise location diagnosed as the source of arrhythmia. In the preferred embodiments as an implantable medical device the electrode array slips over the heart as a sleeve covering the heart surface in part or its entirety. In preferred embodiments, the device may have internal circuitry capable of processing the diagnostic information, determining the appropriate therapy configuration, and subsequently delivering the appropriate electrical stimulation to the site determined as the source of arrhythmia in a manner as to restore normal heart function. In preferred embodiments, the device may also wirelessly transmit information (diagnostic information, record of device activity etc.,) to an external source. In preferred embodiments, the device may also wirelessly receive information (patient information, therapy treatment options etc.,) from

the external source.

Chapter 4: Conclusion

4.1 Discussion

The thesis has described the clinical significance, and pathophysiology of Atrioventricular Nodal Reentry Tachycardia, examined the current state of clinical practice for how the disease is treated and with what devices it is treated. This thesis also evaluated the constraints present in current technologies and introduced new technologies developed by Dr. John Roger's lab at the University of Illinois Urbana in collaboration with the Igor Efimov lab at George Washington University with promise of new treatment options highlighting the new capabilities that such new technologies give rise to and the new limitations that come with them. Finally, this thesis proposed a novel device to be used in the treatment of AVNRT. The proposal included the requirements for that device, and provide a design specification for how to achieve those requirements. The finished device is incomplete in that it requires physical testing verification, validation and trials to ensure that the specifications detailed can achieve the intended therapeutic effect. However, the specifications in this thesis provide a significant starting platform from which to further develop the technology for use in AVNRT or for the design of a host of devices for the improved treatment of disease states associated with endocardial mapping and ablation.

4.2 Future Work

Though the design specifications meet the requirements, there are several subsequent tasks that can be done to improve upon the design outlined above.

The first set of improvements have to do with the configuration of the circuit board electronics. The PCB arrangement can be further optimized based by the manufacturer of the PCB to rearrange the electrodes and reduce the amount of space that is left unutilized on the surface of the PCB. Currently, 82% of the available space on the PCB is covered by a sensor or electrode the remaining 18% is on the edges of the rows of electrodes where another sensor or electrode could not be placed. Additionally, there are spaces between rows that are created by the taller (560um) being left adjacent to the shorter (500um) sensors. The difference of 60um is unused space. More efficient packing algorithms from PCB manufacturers may be able make better use of the space while still meeting the design requirements.

The pleating design proposed in the specifications is based on a simple pleating arrangement that fulfils the design requirements for fitting the balloon into a catheter. However, manufacturers of balloon pleating machinery often provide custom solution machinery for catheter manufacturers and work alongside them to best incorporate a pleat design. Using a pleating design with input from a manufacturer of the machinery that would be used to perform the pleating could lead to more optimal use of space on the balloon surface and less area devoted to folding space for the catheter.

Another task for future work is the creation of custom software that is able to incorporate the signal data from the mapping sensors, generate a map of the AVNRT aberrant pathway, and direct the correct ablation electrodes to ablate the proper position. Such software is integral to automating the AVNRT ablation

procedure which is the primary focus of this device. In addition to automated sensing and ablation targeting, the software would need to be able to direct one or more electrodes to deliver a pacing rhythm in order to attempt a reinitiating of the reentrant pathway to ensure that the ablation was successful. The software necessary for this pacing would have to be developed for this device. However, in addition, a novel pulse generator with the ability to deliver both high energy, high frequency ablation pulses as well as low energy and lower frequency pacing would have to be generated for the device. The software could utilize correlation algorithms to detect the location of the reentry pathway by using fewer sensors that the number currently placed on the device. Such an algorithm would have to be developed once empirical data showing the multiplexing functions of the sensors and sensitivity of the signal acquisition are gathered in a prototype.

As previously discussed, the chiplet designs would have to be tested in order to evaluate the forces present when the device is flexed about an arc with a 5mm radius. This testing would have to be conducted to ensure that the sensors do not undergo any deformation and that their performance is unchanged. Similar testing for all of the electronics would have to be conducted or reusability testing and for stress testing showing the nominal performance of the device after repeated ablation, sensing and pacing regimens.

All of the future work requires an initial prototype of the device to be constructed so that parameters and specifications of this device can be tested in the context of a catheter where before, they had only been tested in separate

conceptual manners.

Bibliography

1. Glover, Benedict M. and Pedro Brugada. “AV Nodal Re-entry Tachycardia (AVNRT).” Clinical Handbook of Cardiac Electrophysiology. Springer international Publishing, 2016. 199-133.

2. Kurian T, Ambrosi C, Hucker W, Fedorov V V., Efimov IR. Anatomy and electrophysiology of the human AV node. PACE - Pacing Clin Electrophysiol 2010;33:754-762. doi:10.1111/j.1540-8159.2010.02699.x. PMID: 20180918.

3. http://www.vhlab.umn.edu/atlas/right-atrium/triangle-of-koch/index.shtml

4. Van Veen TAB, Van Rijen HVM, Opthof T. Cardiac gap junction channels: Modulation of expression and channel properties. Cardiovasc Res. 2001;51:217-229. doi:10.1016/S0008-6363(01)00324-8. PMID: 11470461.

5. Vozzi C, Dupont E, Coppen SR, Yeh HI, Severs NJ. Chamber-related differences in connexin expression in the human heart. J Mol Cell Cardiol. 1999;31:991-1003. doi:10.1006/jmcc.1999.0937. PMID: 10336839.

6. Revel JP, Yancey SB, Nicholson B, Hoh J. Sequence diversity of gap junction proteins. Ciba Found Symp. 1987;125:108-127. PMID: 3030671.

7. Boyett MR, Inada S, Yoo S, et al. Connexins in the sinoatrial and atrioventricular nodes. Adv Cardiol. 2006;42:175-197. doi:10.1159/000092569. PMID: 16646591.

8. Inoue S, Becker a. E. Posterior Extensions of the Human Compact Atrioventricular Node : A Neglected Anatomic Feature of Potential Clinical Significance. *Circ 1998;* 97:188-193. doi:10.1161/01.CIR.97.2.188. PMID: 9445172.

9. Medkour D, Becker a E, Khalife K, Billette J. Anatomic and functional characteristics of a slow posterior AV nodal pathway: role in dual-pathway physiology and reentry. *Circulation*. 1998;98:164-174. doi:10.1161/01.CIR.98.2.164. PMID: 9679723.

10. Hucker WJ, McCain ML, Laughner JI, Iaizzo PA, Efimov IR. Connexin 43 expression delineates two discrete pathways in the human atrioventricular junction. *Anat Rec*. 2008;291:204-215. doi:10.1002/ar.20631. PMID: 18085635.

11. Chiou CW. Effects of Continuous Enhanced Vagal Tone on Dual Atrioventricular Node and Accessory Pathways. *Circulation*. 2003;107:2583-2588. doi:10.1161/01.CIR.0000068339.04731.4D. PMID: 12743004.

12. Philippon F, Plumb VJ, Kay GN. Differential effect of esmolol on the fast and slow AV nodal pathways in patients with AV nodal reentrant tachycardia. *J Cardiovasc Electrophysiol*. 1994;5:810-817. PMID: 7874326.

13. Fedorov V V., Ambrosi CM, Kostecki G, et al. Anatomic localization and autonomic modulation of atrioventricular junctional rhythm in failing human hearts. *Circ Arrhythmia Electrophysiol*. 2011;4:515-525. doi:10.1161/CIRCEP.111.962258. PMID: 21646375.

14. Nikolski VP, Jones SA, Lancaster MK, Boyett MR, Efimov IR. Cx43 and dual-pathway electrophysiology of the atrioventricular node and atrioventricular nodal reentry. *Circ Res*. 2003;92:469-475. doi:10.1161/01.RES.0000059304.97120.2F. PMID: 12600895.

15. Hucker WJ, Nikolski VP, Efimov IR. Optical mapping of the atrioventricular junction. In:

Journal of Electrocardiology. Vol 38. ; 2005:121-125. doi:10.1016/j.jelectrocard.2005.06.024. PMID: 16226086.

16. Hucker WJ, Sharma V, Nikolski VP, Efimov IR. Atrioventricular conduction with and without AV nodal delay: two pathways to the bundle of His in the rabbit heart. *Am J Physiol Hear Circ Physiol*. 2007;293:H1122--30. doi:10.1152/ajpheart.00115.2007. PMID: 17496219.

17. Wang DW. Clinical, Genetic, and Biophysical Characterization of SCN5A Mutations Associated With Atrioventricular Conduction Block. Circulation. 2002;105:341-346. doi:10.1161/hc0302.102592. PMID: 11804990.

18. Jackman, Warren M., et al. "Treatment of supraventricular tachycardia due to atrioventricular nodal reentry by radiofrequency catheter ablation of slow-pathway conduction." New England Journal of Medicine 327.5 (1992): 313-318.

19. Kuck, Karl-Heinz, et al. "Cryoballoon or radiofrequency ablation for paroxysmal atrial fibrillation." N Engl J Med 2016.374 (2016): 2235-2245.

20. Kusumoto, and Goldschlager. Cardiac pacing for the clinician. Eds. Fred M. Kusumoto, and Nora F. Goldschlager. Springer, 2008.

21.https://www.bostonscientific.com/content/dam/bostonscientific/ep/general/Boston%20Scientific%202014%20Electophysiology%20Products%20Catalog.pdf

22. http://www.medtronic.com/us-en/healthcare-professionals/products/cardiac-rhythm/ablation-arrhythmias.html

23. https://www.biosensewebster.com/products/diagnostics-lasso.aspx

24. https://www.sjm.com/en/professionals/featured-products/electrophysiology/therapy/irrigated-ablation-catheters/tacticath-quartz-contact-force-ablation-catheter?alert=DeepLinkSoftAlert&clset=af584191-45c9-4201-8740-5409f4cf8bdd%3ab20716c1-c2a6-4e4c-844b-d0dd6899eb3a

25. https://www.biosensewebster.com/products/carto-3/smarttouch-catheter.aspx

26. https://www.sjm.com/en/professionals/featured-products/electrophysiology/therapy/irrigated-ablation-catheters/tacticath-quartz-contact-force-ablation-catheter/isw#tabs

27. Wittkampf, Fred HM, Richard Nw Hauer, and EO Robles de Medina. "Control of radiofrequency lesion size by power regulation." Circulation 80.4 (1989): 962-968.

28. Ullah, W., R. J. Schilling, and T. Wong. "Contact Force and Atrial Fibrillation Ablation." Journal of atrial fibrillation 8.5 (2016).

29. Kim, Dae-Hyeong, et al. "Stretchable and foldable silicon integrated circuits." Science 320.5875 (2008): 507-511.

30. Kim DH, Lu N, Ma R, Kim YS, Kim RH, Wang S, et al. Epidermal electronics. Science. 2011;333(6044):838-43.

31. Kim DH, Lu N, Ghaffari R, Kim YS, Lee SP, Xu L, et al. Materials for multifunctional balloon catheters with capabilities in cardiac electrophysiological mapping and ablation therapy. Nature materials. 2011;10(4):316-23.

32. Viventi J, Kim DH, Moss JD, Kim YS, et al. A conformal bio-interfaced class of silicon electronics for mapping cardiac electrophysiology. Science translational medicine. 201o;2(24):24ra2.

33. Kim, D-H. et al. Materials and noncoplanar mesh designs for integrated circuits with linear elastic responses to extreme mechanical deformations. Proc. Natl Acad. Sci. USA 105, 18675–18680 (2008)

34. Viventi, J. et al. A Conformal, bio-interfaced class of silicon electronics for mapping cardiac electrophysiology. Sci. Translational Med. 2, 24ra22 (2010)

35. Xu, Lizhi, et al. "Materials and fractal designs for 3D multifunctional integumentary membranes with capabilities in cardiac electrotherapy." Advanced Materials 27.10 (2015): 1731-1737.

36. https://patents.google.com/patent/WO2014124044A1/en?q=illinois&q=H05K1%2f0283&inventor=John+A.+Rogers

37. Fang, Hui, et al. "Capacitively coupled arrays of multiplexed flexible silicon transistors for long-term cardiac electrophysiology." Nature Biomedical Engineering 1 (2017): 0038.

38. Langendorf, O. Untersuchungen am überlebenden Säugethierherzen. Pfügers Archiv Eur. J. Physiol. 61, 291–332 (1895).

39. Zhivadinovic, J., and D. Lazarova. "Dimensions and muscular architecture of the triangle of Koch." Prilozi 27.2 (2006): 217-224.

40. Yamaguchi, Takanori, et al. "Anatomical and electrophysiological variations of Koch's triangle and the impact on the slow pathway ablation in patients with atrioventricular nodal reentrant tachycardia: a study using 3D mapping." Journal of Interventional Cardiac Electrophysiology 37.1 (2013): 111-120.

41. Machine Solutions. "Machine Solutions Balloon Pleating and Folding Equipment Calalogue", Jan. 2017, https://machinesolutions.com/msi/wp-content/uploads/sites/3/2016/03/FFS760S.pdf.

42. Leon, Martin B., Hemal Gada, and Gregory P. Fontana. "Challenges and future opportunities for transcatheter aortic valve therapy." Progress in cardiovascular diseases 56.6 (2014): 635-645.